COMMUNICATIONS

Influence of Phase-Transport Phenomena on Macrosegregation and Structure Formation During Solidification**

By *Menghuai Wu** and *Andreas Ludwig*

Phase-transport phenomena such as melt convection, sedimentation, and phase separation play a very important role in solidification and structure formation. A two-phase volume averaging model was developed. Simulation results demonstrated that this two-phase model was able to simulate solidification including nucleation, grain evolution, phase transport, solute transport, macrosegregation, and so on. The phase-transport phenomena lead to macrosegregation, and strongly influence the grain-structure distribution. This was evaluated by comparing numerical predictions with experiments. The numerically predicted grain-size distribution in a plate casting (Al–4 wt.-% Cu) was found to agree with experimental analyses. These encouraging results stimulated further studies and improvements to this model.

For a long time industry casting practice and laboratory investigations have demonstrated the importance of phase-transport phenomena such as melt convection, sedimentation or phase separation in solidification, structure, and macrosegregation formation.[1–3] However, only recently it has been possible to model the solidification process and these complicated transport phenomena.[4,5] A new and promising model is the volume-averaging approach developed by Beckermann's group,[5–11] in which solidification is considered to be a multiphase and multiscale problem. This approach was further modified by Ludwig and co-workers for globular equiaxed solidification,[12,13] and some uncertainties appearing in the pioneering model handling of complicated dendritic solidification morphology were avoided.[14,15] This model was recently applied to globular equiaxed solidification in industrial alloys such as Al–4 wt.-% Cu and phase separation in hypermonotectic alloys such as Al–10 wt.-% Bi. Spherical morphology was used for the solidified (or decomposed) primary phase.

[*] *Dr. M. Wu, Dr. A. Ludwig*
Foundry Institute, Aachen University of Technology
Intzestrasse 5, D-52072 Aachen (Germany)
E-mail: menghuai@gi.rwth-aachen.de

[**] *This work was financially supported by the German Science Foundation (DFG) as part of the collaborative research center "Integral Materials Modeling", the ESA-MAP project "Solidification Morphologies of Monotectic Alloys-MONOPHAS", and the DLR project "Simulation of the Dynamics of Monotectic Solidification".*

In order to describe briefly the basic approach of the v ume-averaging method,[12,13] we consider a volume element shown in Figure 1. Convection and sedimentation occur as primary phase nucleates and grows in the melt. The mo ment of the solid phase influences the grain structure distril tion. Owing to solute partitioning at the liquid–solid interfa the average liquid concentration c_l is different from the av age solid concentration c_s; relative movement between the l uid and the solid causes macrosegregation. In the two-ph model considered in this report, the liquid phase and the s ondary phase (solid or second liquid) are treated as separat but coupled and interpenetrating continua. The mass-tra port equations for both phases are written as

$$\frac{\partial}{\partial t}\left(f_l \rho_l\right) + \nabla \cdot \left(f_l \rho_l \vec{u}_l\right) = M_{sl}$$

$$\frac{\partial}{\partial t}\left(f_s \rho_s\right) + \nabla \cdot \left(f_s \rho_s \vec{u}_s\right) = M_{ls}$$

where f_l, f_s are the volume fraction of the liquid and sc phases, ρ_l, ρ_s are the densities. The liquid is transported cording to u_l, and the solid according to u_s. The momentu enthalpy, and species conservation equations that are used determine the other dependent variables such as tempe tures T_l, T_s velocities u_l, u_s, and species concentrations c_l are described elsewhere.[5,12,13,16] Interactions between the t phases such as mass transfer, friction and drag, sol partitioning, and release of latent heat are included in the c responding exchange and source terms. For example, M_{ls} (M_{sl}) in Equations 1 and 2 is the mass-transfer rate.

The grains are also assumed to be transported according u_s. This is taken into consideration by the grain-density c servation equation

$$\frac{\partial}{\partial t} n + \nabla \cdot \left(\vec{u}_s n\right) = N$$

with grain density n, and nucleation rate N. Here, an emp cal three-parameter nucleation law[4] is used. With the kno n and f_s, the average grain size is estimated as

$$d_s = \sqrt[3]{6 f_s / (\pi n)}$$

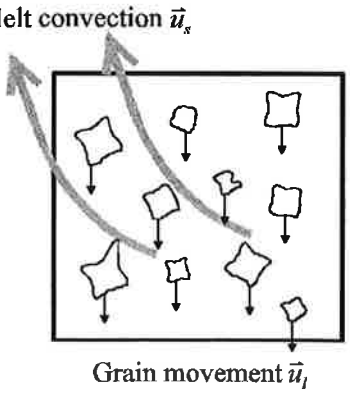

Fig. 1. Diagram of melt convection and grain movement in a volume element.

  1438-1656/03/01–0202-0062 $ 17.50+.50/0

ADVANCED ENGINEERING MATERIALS

As an example to demonstrate the capability of the recent model we present simulation results for an Al–4 wt.-% Cu ingot casting in Figure 2. Using Ti as a grain refiner, the solidification morphology of this alloy is assumed to be globular. The metallic die at a constant temperature (290 K) is assumed to be filled instantaneously with melt (925 K). The heat-exchange coefficient at the casting–mold interface is taken to be 750 W/(m^2 K). An open thermally isolated boundary condition at the casting top is applied, so that hot melt can feed the casting continuously. The nucleation parameters are taken to be $n_{max} = 10^{14}$ m^{-3}, $\Delta T_N = 10$ K, $\Delta T_\sigma = 4$ K.[4] Constant densities for both liquid and solid are used, hence thermal and solutal convection are ignored here. The phase-transport phenomena in this model consider solid sedimentation, sedimentation-induced melt convection, and feeding flow ($\rho_s > \rho_l$). Further details of the problem description and thermal physical properties used are given elsewhere.[12,13,16]

In the initial stage (Fig. 2a) feeding flow caused by solidification shrinkage is dominant. Nucleation and solidification start first in the four corners, and subsequently along the mold walls. The grains nucleated directly on the wall do not move. With further solidification the grains that are not directly adhering to the mold wall sink downwards (Fig. 2b). As the solid and the liquid are coupled through the momentum exchange terms the melt is drawn by the sinking grains, forming two vortices: one clockwise in the right half and one anticlockwise in the left half of the casting. Obviously, at this stage of solidification the sedimentation and the sedimentation-induced melt convection are dominant. Grain settlement occurs as the local f_s exceeds the packing limit $f_s^c = 64$ %. Grain movement leads to the accumulation of solid phase in the lower corner and bottom regions. Grain settlement is responsible for the negative segregation in these areas (zones A and D in Fig. 2). Mechanisms for positive segregations are the feeding of packed zones by segregated melt, and squeezing out of segregated melt by settling grains.[16] The positive segregation zones B are caused by the first mechanism, while zones C are caused by the second. The zones C occur in the bulk melt. They move with the flow current and ascend towards the inner regions of the casting. As shown in Figure 2c, the grain-size distribution along the casting walls is relatively uniform (about 50 μm). Relatively large grains appear in the central region. The solid velocity field indicates that these large grains may have been transported from other regions. The grains nucleated along the vertical walls sink and grow. As they reach the lower central regions, they have grown to a relatively large size. As solidification proceeds the zone of large grains moves upwards, while the grains continue to grow.

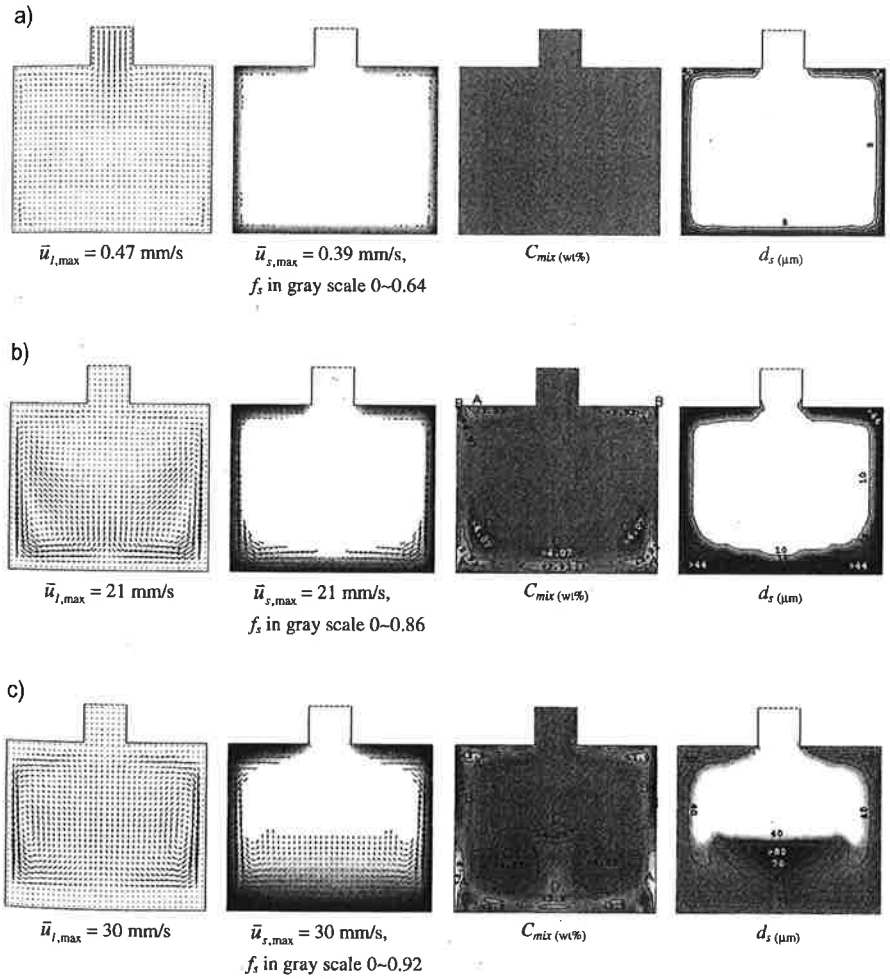

Fig. 2. Solidification process of a 180 mm × 150 mm Al–4 wt.-% Cu ingot casting. The arrows of both velocities are linearly scaled from zero to the maximum value given. The fraction solid f_s is shown together with the solid velocity. c_{mix} and d_s are shown with isolines together with 30 gray levels, with dark showing the highest value and bright the lowest: a) 5 s after cooling starts, b) 16 s after cooling starts, c) 28 s after cooling starts.

Figure 3 shows the simulated solidification process for a hypermonotectic alloy (Al–10 wt.-% Bi) under zero gravity conditions. The two-phase model used is similar to that for the globular equiaxed solidification. The minority liquid phase (Bi), decomposed from the parent melt as droplets in the miscibility gap, is treated as the second phase L_2, while the parent melt is the first phase L_1. The morphology of the decomposed second phase is assumed to be ideally spherical. The thermocapillary (Marangoni) motion of the second phase droplets is modeled by considering an additional source term in the momentum conservation equations: the volume-averaged Marangoni force F_M.[17]

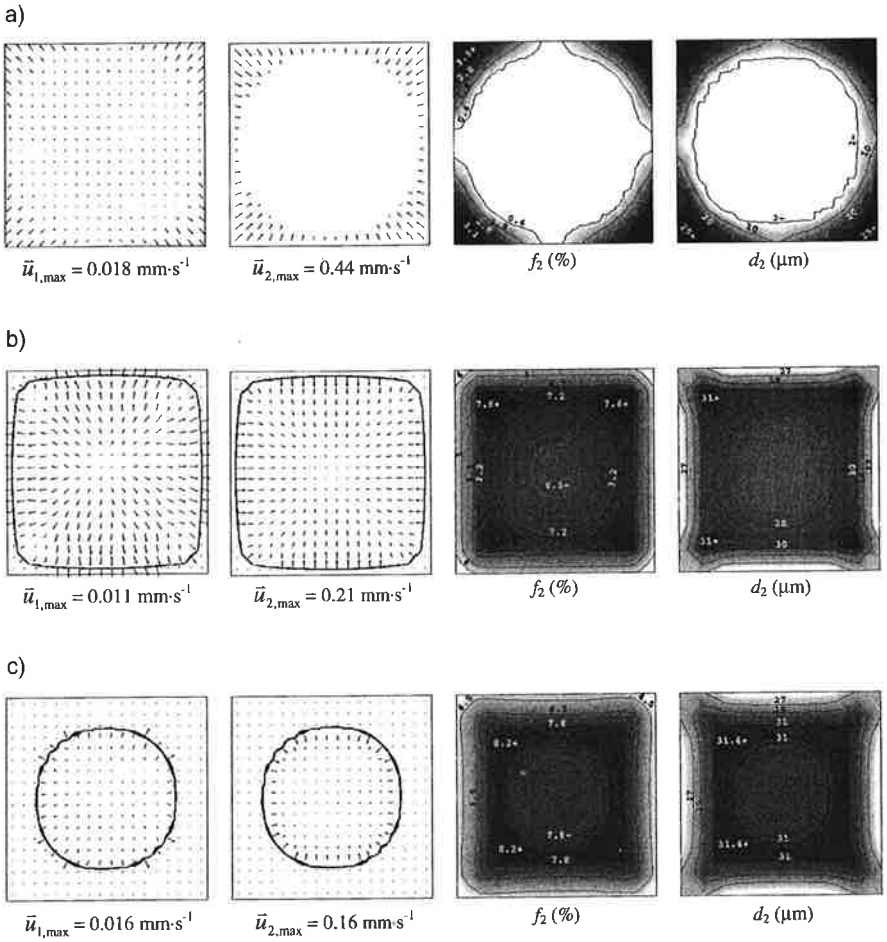

Fig. 3. Solidification process of a 90 mm × 90 mm square casting with a hypermonotectic alloy Al–10 wt.-% Bi under zero-gravity conditions. The arrows of both velocities are linearly scaled from zero to the maximum value given. The monotectic reaction front (T = 930 K) is also drawn together with the velocity field. All other quantities are shown with isolines together with 30 gray levels, with dark showing the highest value and bright the lowest: a) 5 s after cooling starts, b) 30 s after cooling starts, c) 70 s after cooling starts.

The thermocapillary force on a single droplet was solved analytically by Young and co-workers.[18–20] The thermocapillary forces acting on all the droplets were integrated and then averaged over the volume element to get the source term F_M. The monotectic reaction is modeled by adding the latent heat to the first phase L_1 and applying an artificially enlarged viscosity to the solidified monotectic matrix in order to model its drastically reduced flowability on solidification. To test the recent model, a simple 2D square casting is simulated. The mold is assumed to remain at a constant temperature (290 K). The heat-exchange coefficient at the casting–mold interface is taken to be 750 W/(m^{2}K). The nucleation parameters are taken as $n_{max} = 10^{13}$ m^{-3}, $\Delta T_N = 20$ K, $\Delta T_\sigma = 8$ K.[4] For other thermal physical properties we refer to literature.[3,21–23] As shown in Figure 3, phase separation occurs even without gravity. The only mechanism that causes this phase transport is Marangoni motion. Droplets of L_2 start to nucleate and grow at the casting surface as the local temperature drops below the binodal. The temperature gradient causes the movement of L_2 droplets from the surface region towards t casting center. The parent melt mov in the reverse direction, because t space of the leaving phase L_2 must filled by the parent melt L_1. The mov ment of L_2 from the corners and fr the surface regions towards the ca ing center will result in a decrease L_2 volume fraction f_2 in the corn and surface regions and an increase the casting center. As the casti further cools down to the monotec point, the monotectic reaction occu Thus, the velocity of L_1 vanishes a the L_2 droplets are trapped in monotectic matrix. Final solidificati results show that the amount of phase is low in the surface regi and high in the inner region. Ph separation is directly responsible the macrosegregation. Both Maran ni motion and diffusion-control growth contribute to the unev droplet size distribution. A tende of finer droplets in the surface regi and relatively large droplets in central region is predicted.

At present we are working furt on this model to include

- the free surface formed at the c ing top or the concentrated pc in the casting due to the solidifi tion shrinkage;
- thermal and solutal convection
- reliable nucleation and gr growth parameters;
- collision and coagulation, which are important in hyp monotectic solidification;
- the parallel computing technique to extend the calculat from 2D to 3D.

Despite the model assumptions needing further impro ments, evaluation efforts were made by comparing numer predictions with a special experimental situation. Figu shows the simulated grain-size distribution in a section o Al–4 wt.-% Cu plate casting, compared with the experime results. The globular equiaxed model was used for the si lations. The mold temperature was taken to be 573 K and heat-exchange coefficient at the casting–mold interface 800 W/(m^{2}K). A convection heat-exchange boundary co tion on the top surface of the casting was applied, the con tion heat-transfer coefficient was taken as 50 W/(m^{2}K), the environmental temperature as 283 K. Solidifica shrinkage and thermal and solutal convection are ignored this case, but sedimentation and sedimentation-induced c vection were considered with the Boussinesq approach. S

ADVANCED ENGINEERING MATERIALS

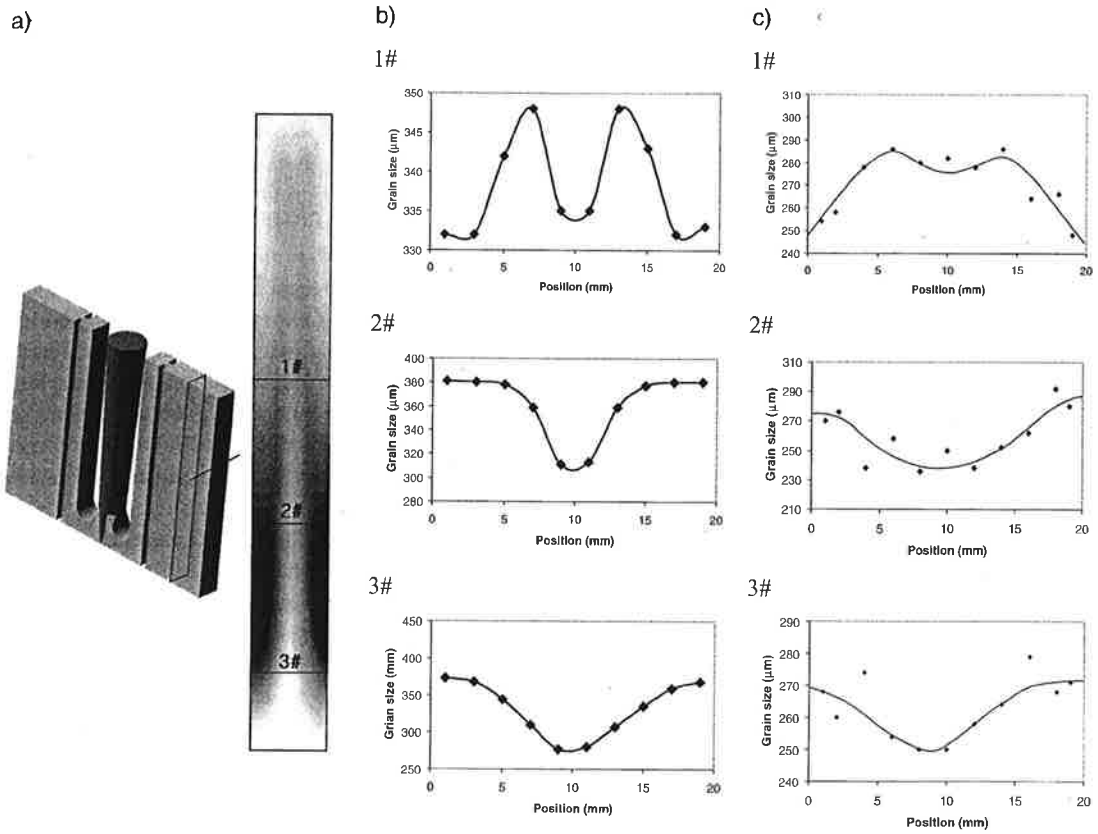

Fig. 4. Comparison of the numerically predicted grain-size distribution in an Al–4 wt.-% Cu plate casting with the experimentally measured results. The nucleation parameters for simulation are $n_{max} = 1.5 \times 10^{12}$ m^{-3}, $\Delta T_N = 20$ K, $\Delta T_\sigma = 8$ K [4]. a) Simulation made in a vertical section of the casting. The grain-size distribution is shown with 30 gray levels, with light showing the smallest grains (262 μm), and dark the largest (390 μm). b) Simulated grain-size distribution across the considered section at three different positions: 1, 2, and 3. c) The experimental casting is sectioned, and the grain-size distribution at the corresponding positions 1, 2, and 3 are metallographically analyzed.

mentation and sedimentation-induced flow currents, similar to the results shown in Figure 2, are also observed in the considered cross section of the plate casting: two vortices occur, one clockwise in the right part and one anticlockwise in the left part of the section. The numerically predicted grain-size distribution across the section of the plate casting is shown in Figure 4a. The fine grain size (about 262 μm) in the bottom region is mainly due to the high nucleation rate in the initial stage, and partially due to sedimentation. The largest grains (about 390 μm) are predicted near the surface regions about 30–40 mm above the bottom. Those large grains are actually transported from the upper regions. They nucleate in the upper region. They sink and grow. As they reach lower regions after a relatively long journey, they have grown to a large size. The relatively small grains predicted in the central region are due to melt currents, which transport the fine grains from the bottom regions upwards to the center. As compared in Figures 4b and 4c, the grain-size distribution in the real casting agrees reasonably with the numerical prediction. The absolute values of the grain sizes are somewhat different between the numerical simulation and the experiment, but the distribution is similar. The casting section was also energy dispersive X-ray (EDX) analyzed for macrosegregation. The experimentally measured data are relatively scattered. It is difficult to fit the experimental data to the numerical results quantitatively. However, the measured result shows the same tendency as the simulation. There is a lower concentration in the bottom region and a higher concentration in top region. Considering the simplifications made in the present model, we find the above agreement between the simulation and the experiment encouraging.

The present model approach can be further developed as a tool for simulating the solidification process including nucleation, grain evolution, melt convection, sedimentation, phase separation, macrostructure, and segregation formation.

Received: July 22, 2002
Final version: September 25, 2002

[1] A. Ohno, *Solidification—The Separation Theory and its Practical Applications*, Springer, Berlin **1987**.
[2] J. Campbell, *Castings*, Butterworth–Heinemann, Oxford **1991**.
[3] L. Ratke, S. Diefenbach, *Mater. Sci. Eng.* **1995**, *15*(R), 263.
[4] M. Rappaz, *Int. Mater. Rev.* **1989**, *34*, 93.

[5] C. Beckermann, R. Viskanta, *Appl. Mech. Rev.* **1993**, *46*, 1.
[6] J. Ni, C. Beckermann, *Metall. Trans.* **1991**, *22B*, 349.
[7] C. Y. Wang, C. Beckermann, *Metall. Mater. Trans. A* **1996**, *27*, 2754.
[8] C. Y. Wang, C. Beckermann, *Metall. Mater. Trans. A* **1996**, *27*, 2765.
[9] C. Y. Wang, C. Beckermann, *Metall. Mater. Trans. A* **1996**, *27*, 2784.
[10] C. Beckermann, *JOM* **1997**, *49*, 13.
[11] A. V. Reddy, C. Beckermann, *Metall. Mater. Trans. B* **1997**, *28*, 479.
[12] A. Ludwig, G. Ehlen, M. Pelzer, P. R. Sahm, in *Proc. McWASP IX*, SIM2000, Shaker, Aachen **2000**, p. 175.
[13] A. Ludwig, M. Wu, G. Ehlen, P. R. Sahm, *Materials Week* **2000**, *Sept*, 25.
[14] J. Ni, F. P. Incropera, *Int. J. Heat Mass Transfer* **1995**, *38*, 1271.
[15] J. Ni, F. P. Incropera, *Int. J. Heat Mass Transfer* **1995**, *38*, 1285.
[16] A. Ludwig, M. Wu, *Metall. Mater. Trans. A* **2002**, *33*, in press.
[17] M. Wu, A. Ludwig, L. Ratke, *McWASP X*, Destin, Florida, 25–30 May, **2003** (in press).
[18] N. O. Young, J. S. Goldstein, M. J. Block, *J. Fluid Mech.* **1959**, *6*, 350.
[19] W. Günter, *Über die Dynamik von Fluidpartikeln aufgrung des Marangoni-Effektes*, DDI, Düsseldorf **1993**.
[20] M. G. Velarde, in *Materials and Fluids under Low Gravity*, (Eds: L. Ratke, H. Walter, B. Feuerbacher), Springer, Berlin, **1995**, p. 283.
[21] S. Diefenbach, *Ph.D. Thesis*, Ruhr University Bochum, **1993**.
[22] F. Falk, in *Immiscible Liquid Metals and Organics* (Eds: L. Ratke), DGM Informationsgesellschaft Verlag, Oberursel **1993**, p. 93.
[23] L. Ratke, S. Dree, S. Diefenbach, B. Pronz, A. Ahlborn, in *Materials and Fluids under Low Gravity* (Eds: L. Ratke, H. Walter, B. Feuerbacher), Springer, Berlin **1995**, p. 115.

On the Behavior of Hot Crack Formation During Solidification in Fe–Ni Alloys**

By *Karin Hansson** and *Hasse Fredriksson*

Abstract: High temperature tensile properties during sol
ification have been determined for two Fe–Ni alloys, in or
to understand the hot cracking (tearing) mechanism. Ten
tests were made on "in situ" solidified samples. Hot crack
susceptibility was determined by using the transition temp
ature for area reduction (hot ductility), i.e. the transition te
perature between a brittle and a ductile fracture. True str
and ultimate tensile stress were also measured. The resu
from the tensile tests were compared to the liquidus and s
dus temperatures, which were measured by thermal analy
using differential scanning calorimetry (DSC).

The Fe-2 %Ni alloy solidifying in the ferritic mode, was
particular sensitive to hot cracking because the transit
temperature for area reduction (ductility) occurred just bel
the solidus temperature. The cooling rate had a minor ef
on the transition temperature. Primarily intergranular fr
tures were formed in the alloy when it solidified to ferrite.

The Fe-10 %Ni alloy solidifying in the austenitic mo
was very sensitive to hot cracking as the transition tempe
ture for area reduction (ductility) was found at 1275–130
at the lowest cooling rate of 10 °C/min. This is about 20
below the solidus temperature. The cooling rate had a str
effect on the transition temperature for area reduction.
creasing cooling rate (100 °C/min) increased the transit
temperature by 100 °C to 1375–1400 °C. The fracture mod
the alloy solidifying to austenite was also dependent on
cooling rate. The low cooling rate gave intergranular fractu
with visible grains, while the medium cooling rate gave in
dendritic fractures with visible dendritic structure. The
perimental results could not be explained by the formatio

[*] *Dr. K. Hansson, Prof. H. Fredriksson*
Department of Production Engineering
Div. of Casting of Metals, Royal Institute of Technology
S-100 44 Stockholm (Sweden)
E-mail: hassef@matpr.kth.se

[**] *This work was supported by the Swedish Research Counci
Engineering Sciences. Thanks to Dr. Mikhail Droujet
Faculty of research of materials, Department of Casting,
Petersburg State Technical University, St. Petersburg, for
with the experimental work on the Fe-10 %Ni alloy and s
of its evaluation. Thanks also to Tomas Antonsson, Dep
Materials Processing, KTH, Stockholm for help with the t
mal analysis.*

  1438-1656/03/01–0202-0066 $ 17.50+.50/0